Study of low-dimensional magnetism in zeolitic imidazolate frameworks

Liliia Kotvytska[1*], Róbert Tarasenko[1], Ralf Feyerherm[2], Slavomír Gabáni[3], Oleksiy Lyutakov[4], Mariia Erzina[4], Olha Vinnik[1], Martin Orendáč[1,2], Alžbeta Orendáčová[1]

[1]Institute of Physics, P. J. Šafárik University, Park Angelinum 9, 04001 Košice, Slovakia

[2]Helmholtz Center Berlin, Hahn Meitner Platz 1, 14109 Berlin, Germany

[3]Institute of Experimental Physics, SAS, Watsonova 47, 04001 Košice, Slovakia

[4] Department of Solid State Engineering, University of Chemistry & Technology, Technická 5, Prague 16628, Czech Republic

liliia.kotvytska@student.upjs.sk

Abstract

Applying the procedure of a rapid synthesis in the aqueous system, nanocrystalline form of ZIF-8 and Cu-ZIF was obtained. The composition of the latter was inferred from the comparison of vibration spectra and lattice specific heats of both compounds which become nearly identical. The nanocrystalline character of both compounds prevented direct comparison of powder XRD spectra and manifested by the appearance of a boson peak in the diamagnetic ZIF-8 specific heat. The low-temperature magnetic contribution in Cu-ZIF specific heat and a Curie-Weiss tail in low-temperature susceptibility may originate from the effect of surface spins while the round maximum observed in the susceptibility at 135 K indicates the presence of strong low-dimensional correlations with the exchange coupling ~200 K. Corresponding magnetic contribution cannot be observed in the specific heat due to the huge overlap by the high-temperature lattice contribution. Negligible magnetization values at low temperatures correspond to the aforementioned strong antiferromagnetic coupling. Future experimental scenarios are discussed which should provide better understanding of the bulk and surface magnetism in this unique quantum system.

keywords: Zeolitic imidazole frameworks (ZIFs), ZIF-8, Cu-ZIF**,** Heisenberg antiferromagnet, boson peak, surface spins, nanocrystallites

1. Introduction

Zeolitic imidazole frameworks (ZIFs) represent a class of metal–organic frameworks (MOFs) with zeolitic topologies. Their structure is built of 3d transition metal ions connected via organic imidazolate linkers forming a three dimensional (3D) porous framework. Large pore volume, high surface area, high thermal and chemical stability predetermine them as excellent candidates for gas adsorption [1] gas separation [2] and catalysis [3]. The functionalization of imidazolate linkers enables further applications due to variation of pore volume and modifying chemical nature of pores [4]. Besides that, the pore size and geometry can change upon external stimuli such as temperature, mechanical pressure, or guest molecule adsorption. Temperature-induced amorphization of some ZIF crystal structures followed by the recrystallization at higher temperatures was reported for ZIF-1, -3, and -4, while the frameworks ZIF-8, -9, -11 and -14 preserved their crystalline form upon heating up to the temperatures of decomposition [5]. Pressure induced amorphization was reported for ZIFs and can be used for the permanent storage of harmful species. Concerning ZIF-8, the amorphization can be induced by mechanical pressure realized by ball milling [6]. The amorphization process leads to the enhancement of the thermal transport due to increased density and offers many practical applications [7, 8]. The effect of functional group substitution and pressure on the thermal conductivity of ZIF-8 was theoretically investigated in ref. [9]. The guest-host interactions associated with the pore occupancy modify the elastic properties of ZIF-8 [10].

While much attention has been devoted to the investigation of monometallic MOFs, recent studies revealed that compared to monometallic MOFs, bimetallic MOFs can provide better performance in various applications as gas separation, storage, catalysis etc. [11]. Concerning ZIF-8, the Zn-Cu substitution improved catalytic activity [12, 13] and absorption capacity [14, 15]. Various strategies for the preparation of Cu-doped ZIF-8 have been developed and the final products preserve the crystal structure and morphology of ZIF-8 crystals if Cu concentrations are lower than the Zn content. The structural studies of Cu-doped ZIF-8 revealed that if Cu concentration exceeds 50%, the ZIF-8 structure corroborates [12]. Therefore, all experimental investigations have been performed with Cu concentrations below 30%.

Cu(II) ion carries spin 1/2, thus, the Cu-doped ZIF-8 systems should possess additional magnetic properties which have not been in the center of attention until now. Since all the aforementioned Cu concentrations are below the percolation limit, the formation of some kind of

modified paramagnetic phases can be expected. Standard approach begins by the investigation of fully concentrated system and then the gradual dilution can provide information about the development of the magnetic system. Therefore, the main goal of our work is a comparative study of ZIF-8 and a compound with 100% content of Cu ions. Since the exact crystal structure is still not fully solved, for the needs of our work we will refer to it as Cu-ZIF not to be confused with Cu-ZIF-8, denotations of Cu-doped ZIF-8 materials frequently reported in literature.

2. Experimental details

$Zn(NO_3)_2 \cdot 6H_2O$, $Cu(NO_3)_2 \cdot 3H_2O$, and 2-methylimidazole were purchased from Sigma-Aldrich, and used as received. ZIF-8 was prepared following the procedure of rapid synthesis in aqueous system [16]. $Zn(NO_3)_2 \cdot 6H_2O$ (1.17 g) was dissolved in 8 g deionized (DI) water. 2-methylimidazole (22.70 g) was dissolved in 80 g DI water. Both solutions were mixed together. After a short stirring the product was collected by centrifugation and then washed with DI water for several times. White polycrystalline product was dried overnight in vacuum at temperature 90°C. The same procedure was applied for Cu-ZIF: $Cu(NO_3)_2 \cdot 3H_2O$ (0.95 g) was dissolved in 8 g DI water, 2-methylimidazole (22.70 g) was dissolved in 80 g DI water. Both solutions were mixed together. The synthesis produced dark brown powder.

Powder XRD spectra of both compounds were recorded by X-Ray diffraction (XRD) diffractometer PANanalytical X'Pert PRO (Malvern Panalytical, UK), using Cu/Kα radiation, λ = 1.54060 Å. The comparison of powder XRD spectrum of the white product with the spectrum calculated for ZIF-8 confirmed excellent sample identity [17].

The formula unit of ZIF-8 is $Zn(mIm)_2$ (HmIm = 2-methylimidazole) with formula sum ($ZnC_8H_{10}N_4$). ZIF-8 crystallizes in the cubic space group I-43m (217), lattice constant a = 17.012 Å, the number of formula units per unit cell is 12 [18]. Tetrahedral coordination of Zn(II) ion (ZnN_4) is formed by nitrogen atoms from imidazolate linkers. The 3D skelet is built of 4–membered ($Zn_4(mIm)_4$) and 6–membered rings ($Zn_6(mIm)_6$) forming pores with the effective diameter about 12.5 Å, the effective hexagonal window size is about 3.3 Å [18].

Concerning Cu-ZIF, the comparison of powder XRD spectrum with that of ZIF-8 indicates realization of different structure (Fig.1). This result coincides with the conclusions of previous studies [12] which revealed that the ZIF-8 structure is not stable for Cu(II) concentrations higher than 50%.

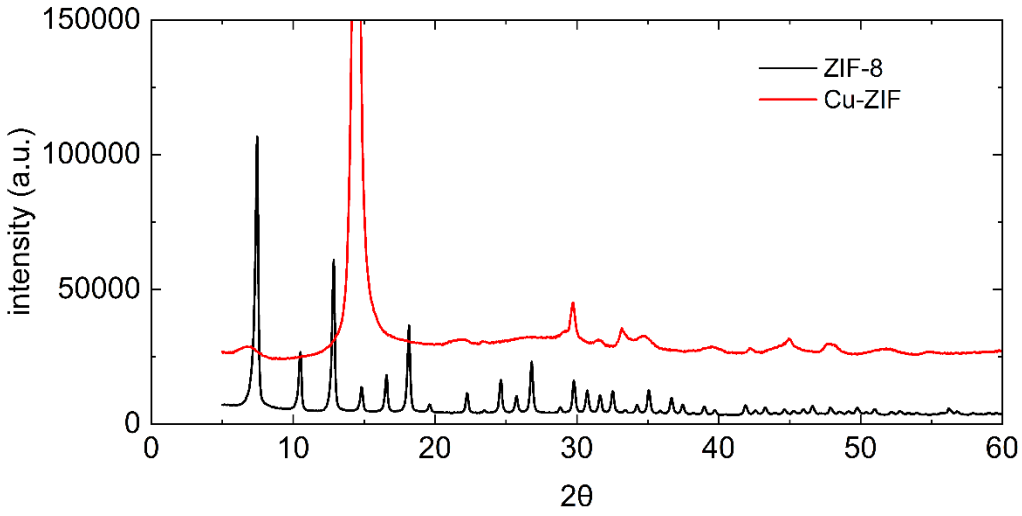

Fig. 1 XRD patterns of ZIF-8 sample and Cu-ZIF sample.

The peaks in the Cu-ZIF XRD spectrum are wider suggesting smaller size of crystallites. Their effective size has been estimated using Scherrer equation $d = K\lambda/(\beta cos\theta)$, where K= 0.9, λ, β and θ stand for X-ray wavelength, full width at half maximum of the most intensive peak and the Bragg angle, respectively. The calculation provided the average size of nanocrystallites ~10 nm for Cu-ZIF and ~30 nm for ZIF-8.

The Raman spectra were recorded on the ProRaman-L spectrometer with 785 nm excitation wavelength with the power density ~345 μW/μm^2 and accumulation time 300 s. The Bruker vacuum FTIR spectrometer, model VERTEX 80 v was used for recording infrared spectra. In the far infrared (FIR) and mid-infrared (MIR) region polyethylene and KBr pellets were used, respectively.

While the XRD spectra are different, the vibration spectra of both compounds are nearly the same (Figs. 2, 3) implying the composition for Cu-ZIF formula unit as Cu(mIm)$_2$ which will be further applied in the analysis of thermodynamic data.

Temperature and magnetic field dependence of magnetic moment (sample mass m = 20 mg) were performed in two devices Magnetic Properties Measurements System, MPMSXL-5 and MPMS3, Quantum Design in the zero-field cooling (ZFC) and field-cooling (FC) regime at temperatures from 2 to 300 K and magnetic fields up to **7** T. Specific heat of powder samples was investigated using Physical Properties Measurements System, Quantum Design, equipped with

He3 insert. The contribution of addenda was measured in a separate run. The measurements were done at temperatures nominally from 0.4 to 300 K and magnetic fields up to 9 T. Polycrystalline samples were manually pulverized, then pressed to a pellet. Then appropriate piece of the pellet was selected for specific heat measurements.

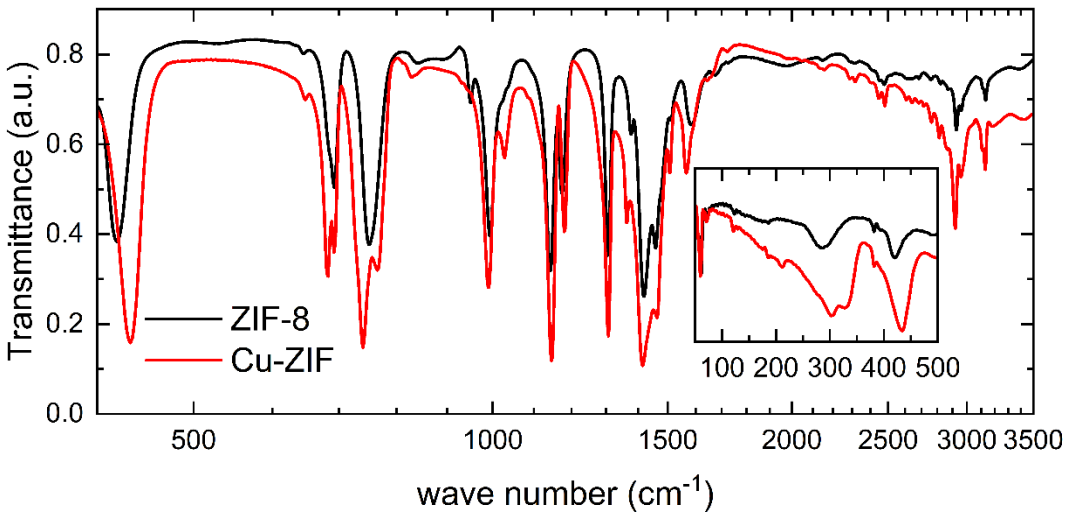

Fig. 2 Comparison of infrared powder spectra of ZIF-8 and Cu-ZIF.

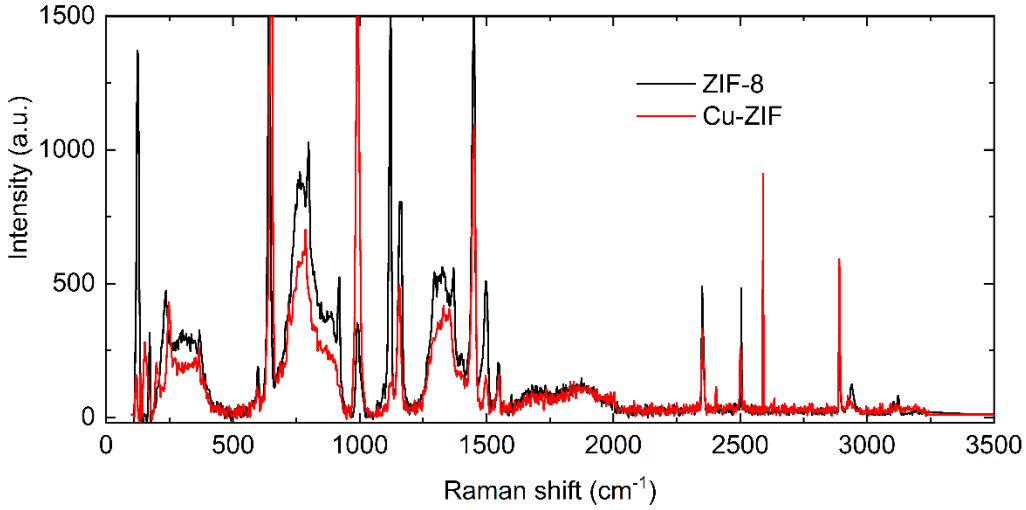

Fig. 3 Comparison of Raman powder spectra of ZIF-8 and Cu-ZIF.

3. Results and discussion

3.1 Specific heat

Previous studies of specific heat of ZIF-8 were performed in zero magnetic field and at temperatures from 2 to 300 K [17]. The analysis of low-temperature specific heat revealed significant deviations from Debye T^3 law. Instead of a constant behavior, the specific heat data divided by T^3 formed a round peak at about 3.5 K [17]. To inspect this behavior in detail, we measured the specific heat in the region from 0.4 to 6 K. Corresponding temperature dependence of C/T^3data is characterized by a round maximum resembling a boson peak characteristic for amorphous and other disordered systems [19]. What is more, a growth of the data below 2 K resembles the glassy behavior as a result of tunneling states in two-level systems describing the physics of glasses at subkelvin temperatures (Fig. 4). Such glassy features in the ZIF-8 crystalline material (Fig. 1) may originate from the process of pellet preparation accompanied with pulverization and effect of mechanical pressure. In future, it would be desirable to perform a control XRD record from the pellets to verify/exclude the effect of such mechanical manipulation on the ZIF-8 structure. The data were fitted by the prediction for soft potential model (SPM) which includes the effect of two-level systems ($C_{\mathrm{TLS}}T$) as well as the contribution of soft modes – the vibrational excitations from single-well soft potentials ($C_{\mathrm{SM}}T^5$) and finally acoustic modes (bT^3) [20]. The fitting by corresponding formula $C_{\mathrm{TLS}}T + bT^3 + C_{\mathrm{SM}}T^5$ provided the best agreement for the C_{TLS}, b and C_{SM} parameters equal to 0.0030 J/K^{2}mol, 0.0067 J/K^{4}mol and $8.3987\cdot10^{-5}$ J/K^{6}mol (Fig. 4). The value of the parameter b is close to the previously estimated 0.0068 J/K^{4}mol providing acoustic Debye temperature 66 K [17]. Such low value indicates the softness of the crystal structure.

Heat capacity of Cu-ZIF was measured in the temperature region from 0.4 to 300 K. In the first step the data were recalculated per gram (denoted as $C^{\text{Cu-ZIF}}$) and compared with the heat capacity of ZIF-8 [17] also recalculated per gram (denoted as $C^{\text{ZIF-8}}$). The recalculated data are depicted in Fig. 5. The comparison of both data sets supports our conjecture about the formula unit for Cu-ZIF which should provide the molar weight $M^{\text{Cu-ZIF}}$= 225.66 g/mol while $M^{\text{ZIF-8}}$ = 227.49 g/mol. The ratio $M^{\text{ZIF-8}}/M^{\text{Cu-ZIF}}$ = 1.008 suggests that also molar specific heats might be the same. Thus, expecting their equality, then the ratio of the heat capacities recalculated per gram should be equal to the aforementioned molar ratio. As can be seen from the inset of Fig.5, the hypothetic molar ratio changes between 0.96 and 0.99. Closer look at the temperature development of the

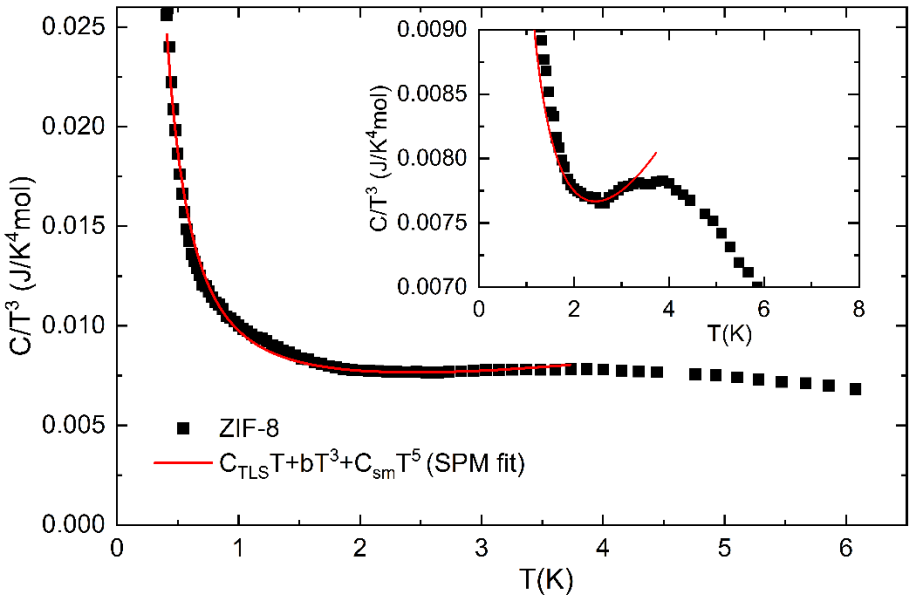

Fig. 4 Temperature dependence of specific heat of powdered ZIF-8 sample divided by T^3. The solid line represents the fit by the prediction of soft potential model. Inset depicts a fragment of the main plot to show better the formation of a boson-like peak.

molar ratio revealed that approximately below 100 K the average value is about 0.97 while at higher temperatures, the average ratio increases to 0.985. The increase may be associated with the fact that at higher temperatures only actual lattice heat capacities of both compounds are compared since at lower temperatures magnetic contribution can be expected in Cu-ZIF.

While both heat capacities seem to be (nearly) the same in the wide temperature range, closer look at the data revealed different behavior somewhere below 6 K. ZIF-8 is insulator with only lattice contribution to the specific heat while Cu-ZIF is magnetic insulator, thus the total specific heat is given by a superposition of the lattice C_{latt} and magnetic contributions C_{mag}. The latter is characterized by a round maximum at (0.48 ± 0.03) K (inset of Fig. 5).

In further analysis both heat capacity data sets were recalculated per mole with aforementioned molar weights.

The fitting of the Cu-ZIF specific heat data by the standard equation $C_{tot} = \frac{a}{T^2} + C_{latt}$ where $C_{latt} = bT^3 + cT^5 + dT^7$ and $\frac{a}{T^2}$ describes a high-temperature tail of C_{mag}, was performed with the aim to separate the lattice contribution. The fitting in the interval from 2 K to 10 K did

not yield satisfactory description, probably due to the fact that alike in ZIF-8, there may also exist boson-like peak in the lattice contribution (Fig. 4). Finally, the best agreement was obtained in the temperature range from 4 to 10 K, (i.e. the temperatures above the hypothetical boson peak) for following parameters a = (6.35 ± 0.30) JK/mol, b = (0.0110 ± 0.0002) J/K^{4}mol, c = (-1.01·10^{-4} ± 5·10^{-6}) J/K^{6}mol and d = (4.23·10^{-7}± 3.3·10^{-8}) J/K^{8}mol. It should be mentioned that the fitting of ZIF-8 data with the same formula for C_{latt} in the same temperature region above boson peak provided very similar parameters, namely b = (0.0108 ± 0.0002) J/K^{4}mol, c = (-0.83·10^{-4} ± 5·10^{-6}) J/K^{6}mol and d = (2.8·10^{-7}± 2·10^{-8}) J/K^{8}mol. Apparently, these fits underestimate the Debye temperature ~ 56 K, however, they are fully sufficient for the separation of the lattice contribution from the total specific heat.

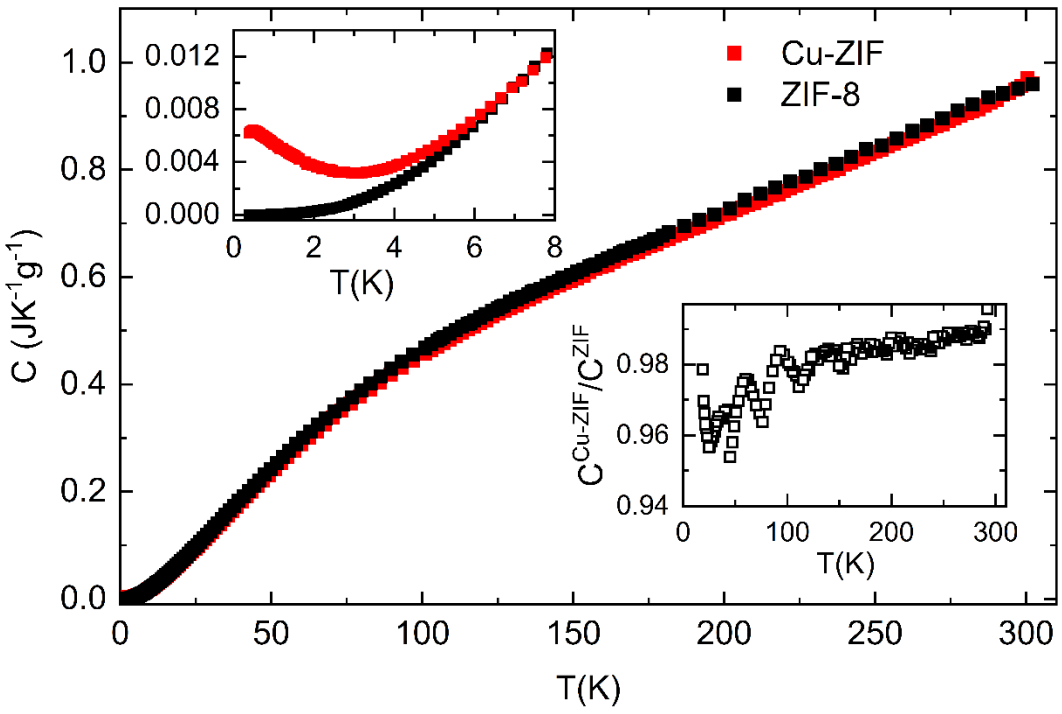

Fig. 5 Temperature dependence of heat capacity of powdered samples of ZIF-8 and Cu-ZIF recalculated per gram. Upper inset: Zoom of the low-temperature part of the main plot. Lower inset: Temperature dependence of the ratio of heat capacities of Cu-ZIF and ZIF-8 recalculated per gram.

Since copper(II) system possesses the spin 1/2, the origin of the round maximum due to the crystal field effects can be excluded. Usually such maximum is formed by short-range magnetic correlations but the onset of long-range order cannot be excluded due to the nano crystallinity of the sample which may cause significant rounding effects. The magnetic entropy associated with the anomaly calculated in the temperature range from 0.4 to 4 K is 2.33 J/Kmol which represents only 40 % of the full *R*ln2 spin entropy, *R* is universal gas constant. The extrapolation from 4 K up to infinite temperatures provides only 0.2 J/Kmol, thus the rest should be hidden at lower temperatures. Even a rough linear extrapolation of the specific heat from 0.4 K down to zero temperature did not bring significant increase of the total magnetic entropy. The missing entropy may imply the presence of additional anomaly somewhere below 0.4 K.

In further step, the development of the round maximum was investigated in magnetic fields up to 9 T. After the separation of lattice contribution, corresponding magnetic specific heats are depicted in Fig. 6. It should be mentioned that the measurements were repeated a few times since

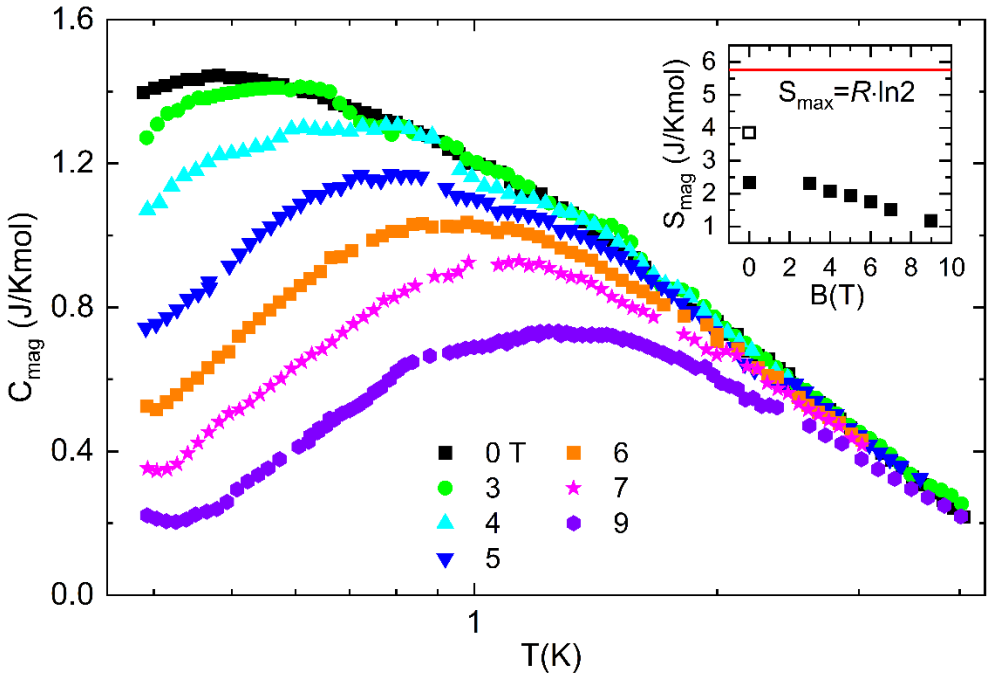

Fig. 6 Temperature dependence of magnetic specific heat of powdered sample of Cu-ZIF in constant magnetic fields. Inset: Development of magnetic entropies in the temperature region between 0.4 and 4 K (full squares). Open square denotes the magnetic entropy in $B = 0$ estimated for the whole temperature range (see text). For the purposes of the entropy calculations the data in 4, 6 and 7 T were extrapolated up to 4 K.

the first experiments provided data which became very noisy below 2 K, as a result of the reduced thermal conductivity probably due to the phonon scattering on the grain boundaries. To improve the measurements, higher pressures were applied in the production of pellets.

In increasing field, the round maximum gradually lowers and shifts towards higher temperatures. This behavior is rather confusing. In the response of standard low-dimensional magnetic systems as spin 1/2 HAF chain or the square lattice [21], the lowering height of the round maximum signals prevailing influence of magnetic correlations up to saturation field. In the vicinity of the saturation field the tendency changes and the saturated phase is characteristic by growing maximum which systematically shifts towards higher temperatures. Apparently, Cu-ZIF data do not preserve such tendency. On the other hand, the upturn of specific heat appearing in our experimental window already in fields above 5 T at lowest temperatures suggests a formation of other anomaly, probably associated with the transition to long range order (Fig. 6). To confirm this conjecture, further specific heat studies are necessary at lower temperatures. Besides that, the magnetic entropy evaluated for each magnetic field in the temperature range from 0.4 to 4 K shows slightly decreasing tendency with increasing field (inset of Fig. 6) which together with the more visible up turns at highest fields suggests the growing portion of the magnetic entropy may be removed below 0.4 K.

3.2 Susceptibility and magnetization

Magnetic susceptibility of Cu-ZIF was measured in the temperature range from 2 to 300 K. The studies were done in the FC and ZFC regimes in constant magnetic fields 10 mT and 1 T, differing by two orders of magnitude. For comparison, magnetic susceptibility of ZIF-8 was measured in the field 1 T in ZFC regime (Fig. 7). Diamagnetic susceptibility of ZIF-8 was calculated $\chi_{dia} = -0.9324 \cdot 10^{-6}$ emu/mol using Pascal constants and was used for the correction of Cu-ZIF data.

A few marked features can be distinguished in the Cu-ZIF data.

The first feature is the appearance of a round maximum with the position at 135 K. In the $S = 1/2$ system, the origin of such maximum could be ascribed to short-range magnetic correlations. Since the maximum is wide and spreads through the whole temperature region, it was not possible to apply fitting with Curie – Weiss law to determine average g-factor and the strength of the low-

dimensional correlations. In the first approximation, the data were compared with the prediction for the S =1/2 HAF chain with g = 2 and intra-chain coupling J/k_B = 225 K (Fig. 7). The excellent agreement indicates the presence of

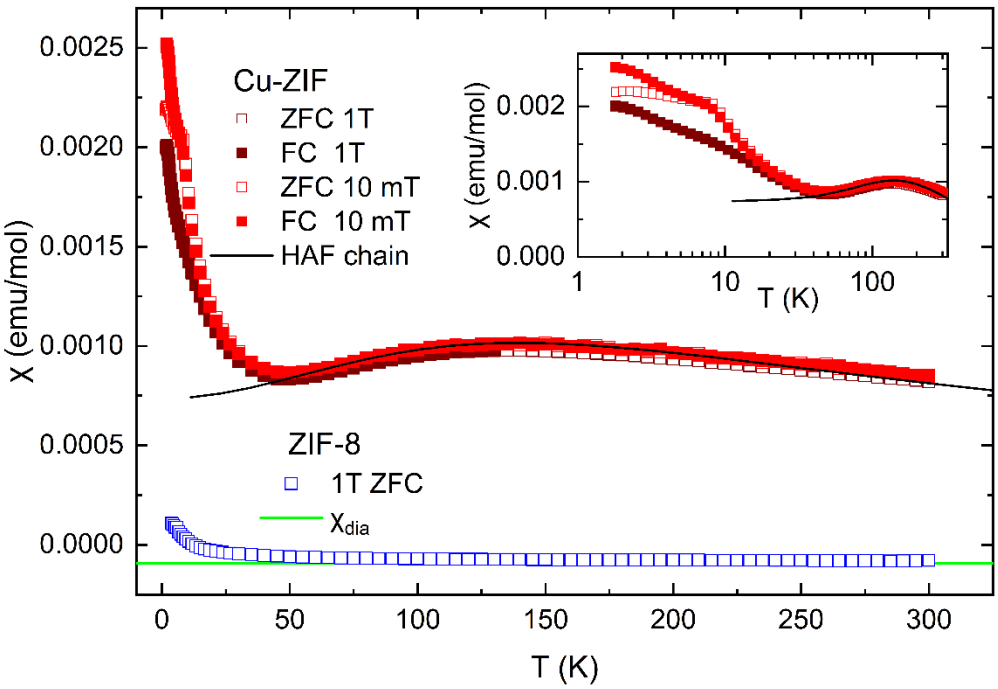

Fig. 7 Temperature dependence of the magnetic susceptibility of powder samples of Cu-ZIF and ZIF-8. The green line represents the diamagnetic contribution calculated for ZIF-8. The black solid line represents the prediction for the S = 1/2 HAF chain with J/k_B = 225 K. Inset: Zoom of the low-temperature part of the main plot, for clarity ZIF-8 data are omitted.

exchange pathways in the Cu-ZIF structure, most probably through the mIm rings, which enable such strong interactions. In future, theoretical calculations of the interaction via the mIm bridge will be performed. The FC and ZFC data are the same in the region of this broad anomaly indicating homogenous character of the antiferromagnetic short-range correlations.

The second feature is a Curie-Weiss tail appearing below 50 K. It should be noticed that much weaker tail appears in the same temperature region also in ZIF-8 data. Considering nanocrystallinity of both materials, the effect of surface spins and/or broken bonds at the surface can be assumed. Depending on the applied field, FC and ZFC data in the tail region are identical in the field 1 T down to lowest temperatures

while those at 10 mK show bifurcation below 6 K. The identity of FC and ZFC data above 6 K suggests that the interactions between the spins are too weak resulting in the effective free spin behavior.

The switching on the couplings between the spins results in the third feature, already mentioned difference between FC and ZFC data below 6 K. It should be noted that the difference between the specific heat of ZIF-8 and CU-ZIF in zero field appears just around the same temperature. Thus, it can be assumed, that the origin of the magnetic specific heat at low temperatures (Fig. 6) comes from the interactions within the surface magnetic subsystem. More detailed quantitative analysis based on the exact knowledge of crystal structure and other material properties will be performed in future studies.

Isothermal magnetization of Cu-ZIF was measured in magnetic fields up to 7 T at temperatures from 2 to 20 K (Fig. 8). The highest values are observed at 2 K and the magnetization gradually lowers with increasing temperature. At temperatures up to about 10 K the curves are nonlinear and the nonlinearity vanishes at higher temperatures, resembling the free spin behavior when thermal fluctuations prevail over the Zeeman energy $g\mu_B B \ll k_B T$.

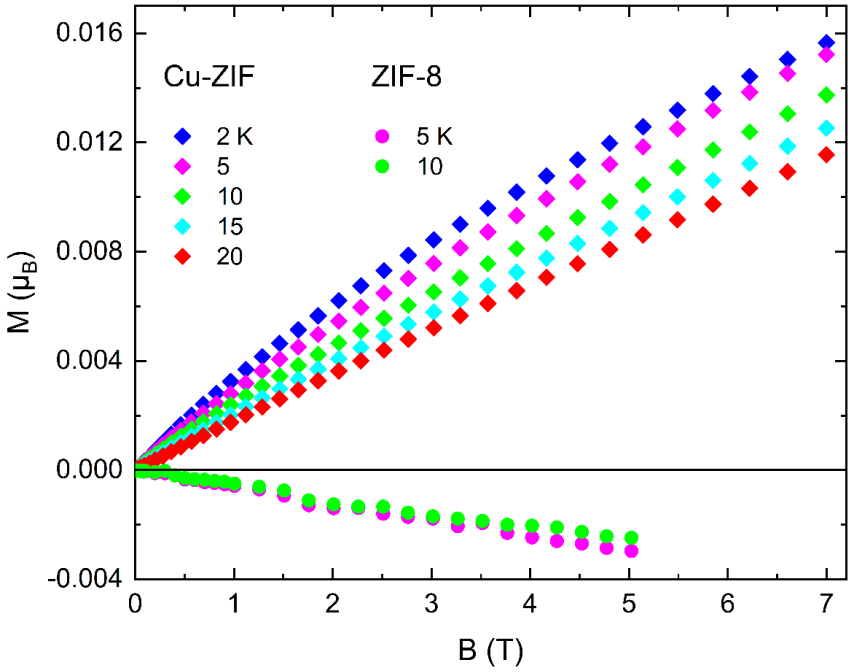

Fig. 8 Magnetic field dependence of the isothermal magnetization of powder Cu-ZIF and ZIF-8.

The most important feature of the Cu-ZIF magnetization is the fact that the data do not achieve saturation value even in the field 7 T. Simple approximation with g = 2 and spin 1/2 provides $M_{sat}/N_A \approx 1\mu_B$ (N_A stands for the Avogadro's constant) while our data at 2 K achieve the highest values ~0.016 μ_B which is only 1.6 % from the saturated value. Considering the large

intra-chain exchange coupling derived from the susceptibility, the ratio of Zeeman energy at 7 T and exchange interaction $h = g\mu_B B/J \approx 0.04$. Quantum Monte Carlo calculations of magnetization of the $S = 1/2$ HAF chain [22] performed at reduced temperature $t = k_B T/J = 0.1$ provide for $h = 0.05$ the magnetization $0.011\mu_B$. For Cu-ZIF the reduced temperature $t = 0.1$ corresponds to 20 K with the magnetization $\sim 0.0115\ \mu_B$. Such closeness of the experimental and theoretical values suggests that the observed magnetization originates from the spins coupled to chains.

In this respect, the question arises, where is the contribution of surface spins. Theoretical calculations of magnetization [22] show linear M vs. B behavior for rather wide range of h which contradicts with the aforementioned nonlinearity in Cu-ZIF data occurring below 10 K. This feature may be associated with the surface magnetization. Since the experimental magnetization is very small, also the magnetization of ZIF-8 was measured to estimate the size of diamagnetic corrections which may become important in this case (Fig. 8). (To avoid experimental errors, the measurements were performed on ZIF-8 pellet without gelcap in the MPMSXL-5 working up to 5 T where a large sample volume does not introduce large experimental uncertainty). The obtained results suggest that the correction for diamagnetic contribution might represent about 20 % from the observed Cu-ZIF magnetization.

To understand the extremely low magnetization, further magnetic studies will be performed in the temperature range where the low-temperature specific heat maxima appear.

4. Conclusions

Cu-ZIF has been prepared following the procedure for the rapid synthesis of porous ZIF-8. The comparison of vibration spectra and lattice specific heat of both compounds revealed very good agreement between the ZIF-8 and CU-ZIF datasets which suggests at least the composition of the basic CU-ZIF formula unit. Powder XRD spectra of both compounds seem to be different. Quantitative analysis of the XRD data is necessary to extract reliable information since the application of Scherrer equation indicates nanocrystalline character of both compounds while the Cu-ZIF nanocrystallites are much smaller. The existence of nanocrystallites with significant surface area may explain the origin of boson peak in ZIF-8 specific heat which is overlapped by a low-temperature magnetic contribution in Cu-ZIF data. Contrary to specific heat, a round

maximum in magnetic susceptibility observed at about 130 K suggests the formation of strong short-range magnetic correlations with exchange coupling ~ 200 K. The strength of the coupling excludes any possibility to observe corresponding magnetic contribution in the specific heat which is overlapped by large lattice contribution at high temperatures. The effect of the surface magnetism probably manifesting in the low-temperature magnetic specific heat is responsible for the low-temperature Curie-Weiss tail in the Cu-ZIF susceptibility. Corresponding magnetization measurements at 7 T can achieve only ~1.5 % of the saturation value, a result of strong antiferromagnetic coupling. For better understanding of this unique magnetic MOF system, many experiments are planned including specific heat studies in mK region, magnetization studies below 2 K completed with the structure analysis, electron paramagnetic resonance spectra and others to separate the manifestation of surface and bulk spins in this quantum magnet.

Acknowledgments

The financial support of projects VEGA 1/0132/22, GAČR 21-025505, DAAD-57561069 and Slovak Research and Development Agency under the contract No. APVV-18-0197 is acknowledged.

References

[1] P. Zhao, G. I. Lampronti, G. O. Lloyd, E. Suard and S. A. T. Redfern, Direct visualisation of carbon dioxide adsorption in gate-opening zeolitic imidazolate framework ZIF-7. J. Mater. Chem. A 2 (2014) 620. https://doi.org/10.1039/C3TA13981F

[2] J. Sánchez-Laínez, L. Paseta, M. Navarro, B. Zornoza, C. Téllez, and J. Coronas, Ultrapermeable Thin Film ZIF-8/Polyamide Membrane for H_2/CO_2 Separation at High Temperature without Using Sweep Gas. Adv. Mater. Interfaces 5 (2018) 1800647.
DOI: 10.1002/admi.201800647

[3] B. Murillo, B. Zornoza, O. de la Iglesia, C. Téllez, J. Coronas, Chemocatalysis of sugars to produce lactic acid derivatives on zeolitic imidazolate frameworks. Journal of Catalysis 334 (2016) 60. https://doi.org/10.1016/j.jcat.2015.11.016

[4] S. Sneddon, J. Kahr, A. F. Orsi, D. J. Price, D. M. Dawson, P. A. Wright, S. E. Ashbrook, Investigation of zeolitic imidazolate frameworks using ^{13}C and ^{15}N solid-state NMR spectroscopy. Solid State Nuclear Magnetic Resonance 87 (2017) 54.

http://dx.doi.org/10.1016/j.ssnmr.2017.09.001
[5] T. D. Bennett, D. A. Keen, J.-C. Tan, E. R. Barney, A. L. Goodwin, and A. K. Cheetham, Thermal Amorphization of Zeolitic Imidazolate Frameworks. Angew. Chem. 123, 3123 (2011). DOI: 10.1002/ange.201007303
[6] S. Cao, T.D. Bennett, D. A. Keen, A. L. Goodwin and A. K. Cheetham, Amorphization of the prototypical zeolitic imidazolate framework ZIF-8 by ball-milling. Chem. Commun. 48 (2012) 7805. DOI:10.1039/c2cc33773h
[7] Y. Zhou, B. Huang, B.-Y. Cao, Vibrational modes with long mean free path and large volumetric heat capacity drive higher thermal conductivity in amorphous zeolitic imidazolate Framework-4. Materials Today Physics 21 (2021) 100516.
https://doi.org/10.1016/j.mtphys.2021.100516
[8] Y. Rao, Z. Kou, X. Zhang, and P. Lu, Metal Organic Framework Glasses: a New Platform for Electrocatalysis? Chem. Rec. (2023) e202200251
doi.org/10.1002/tcr.202200251
[9] P. Ying, J. Zhang, X. Zhang and Z. Zhong, Impacts of the Functional Group Substitution and Pressure on the Thermal Conductivity of ZIF-8. J. Phys. Chem. C 124 (2020) 6274.
DOI: 10.1021/acs.jpcc.0c00597
[10] D. Radhakrishnan and Ch. Narayanaa, Effect of pore occupancy on the acoustic properties of zeolitic imidazolate framework (ZIF)-8: A Brillouin spectroscopic study at ambient and low temperatures. J. Chem. Phys. 143 (2015) 234703.
http://dx.doi.org/10.1063/1.4937763
[11] M. Y. Masoomi, A. Morsali, A. Dhakshinamoorthy, and H. Garcia, Mixed-metal MOFs: unique opportunities in metal–organic framework (MOF) functionality and design.
Angew. Chem. Int. Ed. 58 (2019) 15188. DOI: 10.1002/anie.201902229
[12] A. Schejn, A. Aboulaich, L. Balan, V. Falk, J. Lalevée, G. Medjahdi, L. Aranda, K. Mozet, R. Schneider, Cu^{2+}-doped zeolitic imidazolate frameworks (ZIF-8): Efficient and stable catalysts for cycloadditions and condensation reactions. Catal. Sci. Technol.5 (2015) 1829.
https://doi.org/10.1039/C4CY01505C
[13] A. Ahmad, N. Iqbal, T. Noor, A. Hassan, U. A. Khan, A. Wahab, M. A. Raza, S. Ashraf, Cu-doped zeolite imidazole framework (ZIF-8) for effective electrocatalytic CO_2 reduction. J. CO2 Utilization 48 (2021) 101523.

[14] S. Sun, Z. Yang, J. Cao, Y. Wang, W. Xiong, Copper-doped ZIF-8 with high adsorption performance for removal of tetracycline from aqueous solution. J. Solid State Chemistry 285 (2020) 121219. https://doi.org/10.1016/j.jssc.2020.121219

[15] X. Wang, Y. Zhao, Y. Sun and D. Liu, Highly Effective Removal of Ofloxacin from Water with Copper-Doped ZIF-8. Molecules 27 (2022) 4312.
https://doi.org/10.3390/molecules27134312

[16] Y. Pan, Y. Liu, G. Zeng, L. Zhao and Z. Lai, Rapid synthesis of zeolitic imidazolate framework-8 (ZIF-8) nanocrystals in an aqueous system. Chem. Commun. 47 (2011) 2071.
DOI: 10.1039/c0cc05002d

[17] L. Kotvytska, R. Tarasenko, O. Lyutakov, M. Erzina, N.Tomašovičová, O. Vinnik, M. Orendáč and A. Orendáčová, Physical Properties of Metal–Organic Zeolitic Imidazolate Frameworks. AIP Conference Proceedings 2778 (2023) 040015.
https://doi.org/10.1063/5.0136197

[18] X.-Ch. Huang, Y.-Y. Lin, J.-P. Zhang, and X.-M. Chen, Ligand-Directed Strategy for Zeolite-Type Metal–Organic Frameworks: Zinc(II) Imidazolates with Unusual Zeolitic Topologies.
Angew. Chem. Int. Ed. 45 (2006) 1557. DOI: 10.1002/anie.200503778

[19] V. L. Gurevich, D. A. Parshin, and H. R. Schober, Anharmonicity, vibrational instability, and the Boson peak in glasses. Phys. Rev. B 67 (2003) 094203.
DOI:https://doi.org/10.1103/PhysRevB.67.094203

[20] Yu. M. Galperin, V. G. Karpov, V.I. Kozub, Localized states in glasses, Adv. Phys. 38 (1989) 669. https://doi.org/10.1080/00018738900101162

[21] L. Lederová, A. Orendáčová, R. Tarasenko, K. Karl'ová, J. Strečka, A. Gendiar, M. Orendáč, A. Feher, Interplay of magnetic field and interlayer coupling in the quasi-two-dimensional quantum magnet $Cu(en)Cl_2$: Realization of the spin-1/2 rectangular/zigzag square Heisenberg lattice, Phys. Rev. B 100 (2019) 134416. https://doi.org/10.1103/PhysRevB.100.134416

[22] L. Lederová, A. Orendáčová, J. Chovan, J. Strečka, T. Verkholyak, R. Tarasenko, D. Legut, R. Sýkora, E. Čižmár, V. Tkáč, M. Orendáč, A. Feher, Realization of a spin-1/2 spatially anisotropic square lattice in a quasi-two-dimensional quantum antiferromagnet $Cu(en)(H_2O)_2SO_4$, Phys. Rev. B 95 (2017) 054436. DOI:https://doi.org/10.1103/PhysRevB.95.054436